Chemical Science

EDGE ARTICLE

Predicting thermal expansion in framework compounds using a charge interaction index

Xin Chen,[a] Qilong Gao, [ID] *[a] Kaiyue Zhao,[a] Yongqiang Qiao,[a] Andrea Sanson, [ID] [b] Qiang Sun,[a] Juan Guo,[a] Shogo Kawaguchi, [ID] [c] Erjun Liang [ID] [a] and Jun Chen [ID] [d]

The precise regulation of thermal expansion is a crucial and challenging topic with significant industrial and technological implications. We propose a charge interaction index (CII) to relate thermal expansion to chemical composition. Using $A_2M_3O_{12}$ compounds as a case study, we show the validity of this parameter through experimental verification. Through first principles calculations, the charge density, potential well curves, and Grüneisen parameters of $A_2Mo_3O_{12}$ (where A = Al, Sc, and Y) were extracted. These calculations revealed that the CII value correlates strongly with the transverse thermal vibrations of bridging O atoms and, in turn, the low-frequency phonon modes possessing negative Grüneisen parameters. Three representative component designs, $Sc_{1.6}(MgTi)_{0.2}Mo_3O_{12}$, $In_2Mo_{2.5}W_{0.5}O_{12}$, and $(Al_{0.2}Sc_{0.2}Fe_{0.2}Ga_{0.2}Cr_{0.2})_2W_3O_{12}$, were synthetized. As predicted, synchrotron XRD as a function of temperature showed that $In_2Mo_{2.5}W_{0.5}O_{12}$, which has the minimum CII value, exhibits negative thermal expansion behavior, while $(Al_{0.2}Sc_{0.2}Fe_{0.2}Ga_{0.2}Cr_{0.2})_2W_3O_{12}$, with the maximum CII value, displays positive thermal expansion. This work establishes a simple and effective strategy to engineer thermal expansion properties in open-framework materials through the CII idea.

Introduction

Slight changes in the coefficient of thermal expansion (CTE) of components or equipment can often reduce their performance and lifespan in various industrial and technological fields, such as advanced electronic devices, biomedical materials, or micromechanical components. Negative thermal expansion (NTE) materials offer significant potential in fine-tuning thermal expansion.[1,2] NTE, as a unique physical property, originates from the interplay between the anharmonic effects of chemical bonds and other contributing factors.[3–7] These factors are related to electrons, spins, and phonons, which contribute to the diversity of NTE materials.[8–13] For example, NTE is caused by the magnetovolume effect in magnetic materials, such as Invar alloys like $Fe_{65}Ni_{35}$,[14,15] $Mn_3(Cu_{1-x}Ge_x)N$,[16] and $La(Fe,Si,Co)_{13}$;[17] charge transfer phenomena lead to significant volume contraction in ABO_3-type perovskites such as $BiNiO_3$,[3] or perovskite-like materials such as $LaCu_3Fe_4O_{12}$;[18] in $PbTiO_3$-based compounds spontaneous volume ferro-electrostriction leads to the lattice contraction.[19] The NTE of these materials bears a strong connection to shifts in their electronic structure.

Additionally, low-frequency phonons play a dominant role in open framework NTE compounds, which feature a weak interplay between electronic and lattice degrees of freedom. Examples include ZrW_2O_8,[20] ScF_3,[21] and $Ag_3[Co(CN)_6]$.[22] Compared to NTE compounds driven by electronic structure changes, open framework NTE materials, where low-frequency phonons play a dominant role, have garnered widespread attention due to their broader temperature ranges for NTE. For example, ZrW_2O_8 and $CaZrF_6$ exhibit pronounced isotropic NTE (ZrW_2O_8: 0.3–1050 K; $CaZrF_6$: 10–1173 K);[20,23] MOF-5 has also been found to display a strong NTE behavior (-39.3×10^{-6} K^{-1}, 80–500 K).[24] The precise regulation of thermal expansion is a key topic for achieving various practical applications and remains a challenging problem. In open framework NTE compounds, the primary methods for controlling thermal expansion include chemical substitution and the incorporation of guest molecules or ions.

Chemical substitution stands as the most traditional and commonly employed approach. For instance, the CTE in $ZrV_{2-x}P_xO_7$ decreases as the P content increases.[25] Furthermore, in $MPt(CN)_6$ compounds where M represents Mn, Fe, Co, Ni, Cu, Zn, or Cd, the thermal expansion characteristics are strongly linked to the size of the M^{2+} cation.[26] However, due to constraints such as system compatibility and the ionic radius of substituting elements, chemical substitution is not always effective. Take ZrW_2O_8, a widely researched material, for instance—chemical substitution has only a restricted impact on regulating thermal expansion.[27–29] Furthermore, inserting guest

[a]*Key Laboratory of Materials Physics of Ministry of Education, School of Physics, Zhengzhou University, Zhengzhou, 450001, China. E-mail: qilonggao@zzu.edu.cn*

[b]*Department of Physics and Astronomy, Department of Management and Engineering, University of Padua, Padova I-35131, Italy*

[c]*RIKEN SPring-8 Center, Sayo-gun, Hyogo 679-5148, Japan*

[d]*Beijing Advanced Innovation Center for Materials Genome Engineering, University of Science and Technology Beijing, Beijing 100083, China*

molecules or ions has proven effective for tuning the thermal expansion behavior of fluorides and cyanides. For example, in ScF_3, partial chemical substitution of Sc with Li and Fe can modulate thermal expansion;[30] the CTE of single-network $Cd(CN)_2$ has been adjusted from negative to positive *via* CCl_4 occupancies;[31] similar results also exist in $Fe_3[Co(CN)_6]_2$ by intercalating CO_2.[32] However, it is important to note that these methods are applicable only to specific systems and are generally ineffective in oxides due to their structural characteristics. To date, no documented cases have been found regarding the successful regulation of thermal expansion in oxides *via* these methods. Given that oxides constitute the majority of NTE materials, it is crucial to develop new predictive and control strategies for thermal expansion.

Efforts to accurately design and predict thermal expansion behavior have already begun. For example, Sanson demonstrated that, by adjusting lattice parameters, the single-well potential related to the rotation of atomic polyhedra (or to the transverse atomic vibrations) can be changed into a double-well potential or fourfold anharmonic potential, thereby decreasing or increasing NTE, respectively.[33] Additionally, our group has introduced average atomic volume (AAV) and average effective electronegativity to predict the NTE behavior and phase transition temperatures.[34,35]

As for open framework oxide NTE materials, it is widely accepted that the larger the anisotropy of bridge atom vibrations, or the more prominent the transverse vibrations, the more pronounced the NTE behavior of the material.[36–39] The key point to note here is what determines the ability of bridge atoms to vibrate laterally. Naturally, two factors come to mind. One is the free vibration space of bridge atoms, which can be quantified by the concept of AAV.[34] The second factor is the force exerted by adjacent metal atoms on the bridge atoms, which can be of Coulomb nature. Therefore, we explore whether a strong correlation exists between charge interaction and thermal expansion. Given the flexibility in chemical composition design and the extensive thermal expansion experimental data available, we use the $A_2M_3O_{12}$ family as a case study and propose a Charge Interaction Index (CII) which is somehow correlated with the Coulomb interaction acting on O atoms. The CII value can be controlled by adjusting the chemical composition.

First, the CII values of the $A_2M_3O_{12}$ compounds were calculated to establish the relationship between CII values and CTE. Subsequently, first principles calculations were performed on materials with different thermal expansion behavior, including positive thermal expansion (PTE) ($Al_2Mo_3O_{12}$), weak NTE ($Sc_2Mo_3O_{12}$), and strong NTE ($Y_2Mo_3O_{12}$), to analyze their electronic structures, energies, and phonon vibrations. These calculations helped validate the CII concept from a theoretical perspective. Finally, based on chemical modifications to the A-site, B-site, and high-entropy structures, we designed and synthesized $Sc_{1.6}(MgTi)_{0.2}Mo_3O_{12}$, $In_2Mo_{2.5}W_{0.5}O_{12}$, and $(Al_{0.2}\text{-}Sc_{0.2}Fe_{0.2}Ga_{0.2}Cr_{0.2})_2W_3O_{12}$. The intrinsic thermal expansion and underlying mechanisms were comprehensively analyzed using temperature-dependent synchrotron X-ray diffraction (SXRD).

Results and discussion

In $A_2M_3O_{12}$-based materials, the NTE is typically associated with the transverse vibrations of the bridging O atom, which is excited by low-frequency phonons. Specifically, the larger the amplitude of these transverse vibrations, the more pronounced the NTE.[40,41] In this work, we introduce a new parameter, the "Charge Interaction Index" (CII), to quantify the degree of constraint imposed on the bridging O atoms by the two adjacent metal atoms (Fig. 1a). We acknowledge that this CII does not represent the Coulomb interaction between atoms, as it merely accounts for the total electric charge present. However, it remains a parameter related to the charge interaction and, most importantly, as we will see later, it proves to be highly effective despite lacking a directly interpretable physical meaning. For $A_2M_3O_{12}$, the CII is defined as:

$$\text{CII} = \frac{C_{A-O} + C_{M-O}}{2} \qquad (1)$$

or more precisely as:

$$\text{CII} = -\left[\frac{\sum_i x_i C_{A_i-O}}{2} + \frac{\sum_j y_j C_{M_j-O}}{3} \right] \Big/ 2 \qquad (2)$$

where x_i and y_j represent the fractional content of the ith element at the A-site and of the jth element at the B-site, respectively. By incorporating the form of Coulomb's law ($Z_1Z_2^2/r^2$) into eqn (2),[42] a more specific representation of CII is obtained:

$$\text{CII} = -\left[\sum_i x_i \frac{Z_{A_i}Z_O}{2(r_{A_i} + r_O)^2} + \sum_j y_j \frac{Z_{M_j}Z_O}{3(r_{M_j} + r_O)^2} \right] \Big/ 2 \qquad (3)$$

where Z is the valence state and r is the ionic radius (Table S1).[43] Based on extensive literature data, the CTE values for molybdates and tungstates have been graphed against CII as shown in Fig. 1b (Table S2). The results indicate that the CTE increases with increasing CII, with a critical point distinguishing NTE from PTE emerging at a CII value of about 2.64 Å^{-2}. Even more interestingly, the relationship between the CII and CTE appears to be more effective than that between the AAV and CTE (Fig. S1), thus demonstrating how the CII is truly relevant for predicting thermal expansion behavior.

To reveal the relationship between CTE and CII, first principles calculations have been conducted on $Al_2Mo_3O_{12}$, $Sc_2Mo_3O_{12}$, and $Y_2Mo_3O_{12}$,[44–46] which exhibit large, medium, and small CII values, respectively. As shown in Fig. S2, the charge density of A-site ions is small, indicating that Al, Sc, and Y have nearly lost three valence electrons, and the A–O bonds are characterized by ionic bonding. To compare the strength of the three A–O bonds, the potential wells for the O atoms have been calculated by transversely shifting the O atoms (Fig. 2a). Among the three compounds, the energy change of the Al–O bond is the most significant when the displacement is altered, followed by $Sc_2Mo_3O_{12}$ and $Y_2Mo_3O_{12}$. This means that the shift of the O atom is most difficult in $Al_2Mo_3O_{12}$ and easiest in $Y_2Mo_3O_{12}$. Since NTE is related to the transverse vibrations of O
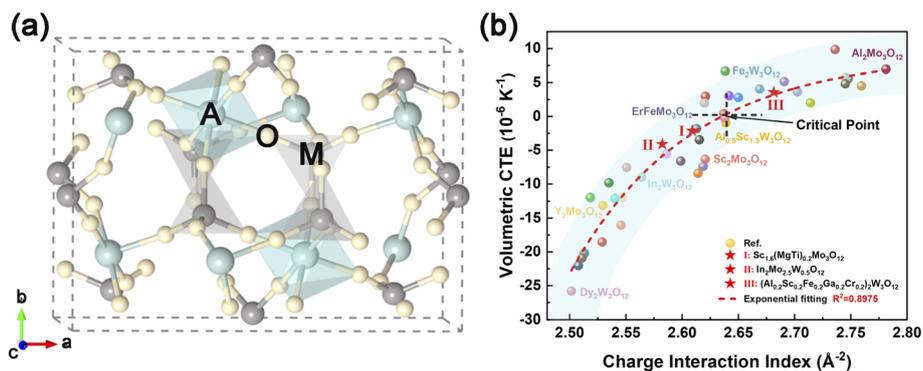
Fig. 1 (a) The crystalline structure of orthorhombic $A_2M_3O_{12}$. (b) Schematic diagram illustrating the relationship between CTE and CII values. The round ball represents the CTE reported in the reference, while the asterisk represents the CTE reported in this study.

atoms, the easier movement of O atoms in $Y_2Mo_3O_{12}$ indicates a greater tendency to exhibit stronger NTE.

The thermal expansion of framework-structured compounds, where phonon contribution to NTE is very important, bears a close connection to the mode Grüneisen parameters (γ_i); the more negative the γ_i are, the greater their contribution to NTE. As depicted in Fig. 2b and c, we derived the γ_i of all phonon modes at zero wave vector and converted them into a point density plot covering the low-frequency range (0–300 cm^{-1}). Compared to $Al_2Mo_3O_{12}$ and $Sc_2Mo_3O_{12}$, $Y_2Mo_3O_{12}$ contains the largest quantity of modes with negative γ_i, leading to the most pronounced NTE. Moreover, the mode of coupling

rotation between polyhedra, which results in NTE in framework materials, exhibits a gradual decrease in frequency from $Al_2Mo_3O_{12}$ to $Sc_2Mo_3O_{12}$ and $Y_2Mo_3O_{12}$ (as shown in the insets of Fig. 2b–d), which is consistent with the difficulty of oxygen atom displacement (Fig. 2a).

To further verify the correlation between CII and CTE, the CII value has been artificially regulated by designing the formula of $A_2M_3O_{12}$. Specifically, the $Sc_{1.6}(MgTi)_{0.2}Mo_3O_{12}$ and $In_2Mo_{2.5}W_{0.5}O_{12}$ compounds were designed and synthesized to investigate the effects of the A-site and M-site, respectively.

For $Sc_{1.6}(MgTi)_{0.2}Mo_3O_{12}$, the orthorhombic structure with a *Pnca* space group was well fitted to the room temperature
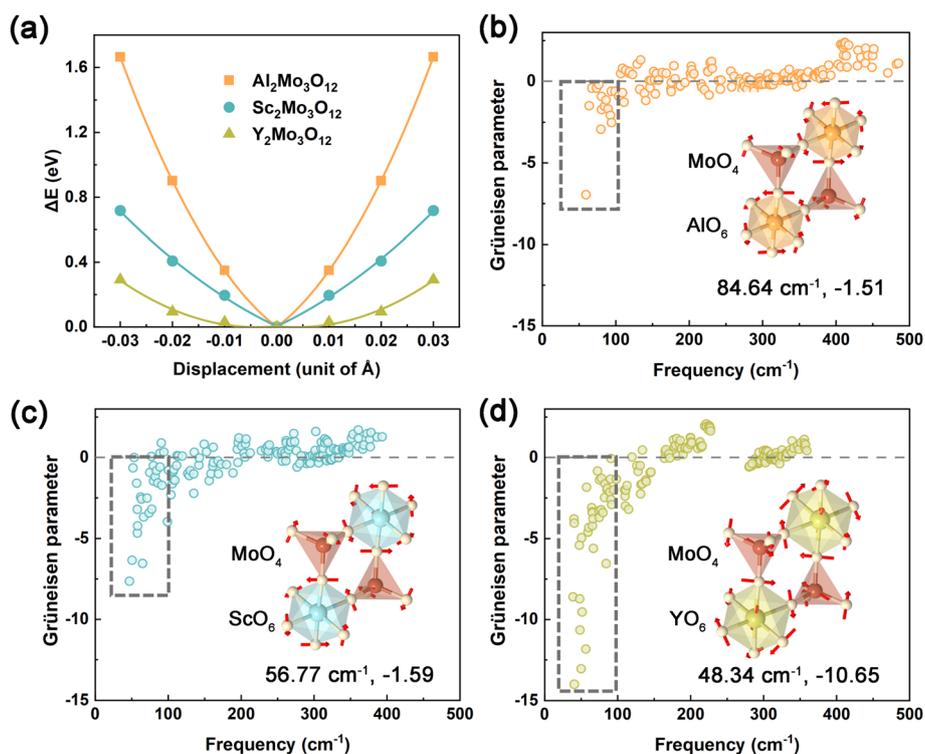

Fig. 2 (a) Potential well of the O atom moving transversely in $A_2Mo_3O_{12}$ (A = Al, Sc, and Y). (b–d) The Grüneisen parameters graphed against vibrational frequency for (b) $Al_2Mo_3O_{12}$, (c) $Sc_2Mo_3O_{12}$, and (d) $Y_2Mo_3O_{12}$. The insets of panels (b)–(d) show the eigenvectors of low-frequency mode related to coupling rotation between polyhedra.

SXRD pattern (Fig. 3a), yielding lattice parameters of $a = 9.5905(2)$ Å, $b = 13.1721(3)$ Å, and $c = 9.4972(2)$ Å, and a unit cell volume of 1199.755(5) Å³ (Table S3). Variable temperature SXRD patterns have been collected from 300 K to 1000 K to extract the intrinsic thermal expansion (Fig. S3), revealing no phase transition across the entire tested temperature range. Anisotropic thermal expansion was observed in $Sc_{1.6}(MgTi)_{0.2}Mo_3O_{12}$ (Fig. 3b), with PTE along the b-axis ($\alpha_b = 6.51 \times 10^{-6}$ K^{-1}) and NTE along the a and c-axes ($\alpha_a = -3.30 \times 10^{-6}$ K^{-1} and $\alpha_c = -5.32 \times 10^{-6}$ K^{-1}). Overall, a zero thermal expansion (ZTE) behavior was achieved, with a volumetric CTE (α_v) of -2.11×10^{-6} K^{-1} over the range of 300–1000 K. Notably, the ZTE temperature range of $Sc_{1.6}(MgTi)_{0.2}Mo_3O_{12}$ exhibits significant advantages over that of many known ZTE compounds, such as

$Mn_3Fe_{0.2}Co_{0.2}Ni_{0.2}Mn_{0.2}Cu_{0.2}N$ (0.72×10^{-6} K^{-1}, 10–180 K),[47] $CoHfF_6$ (-1.32×10^{-6} K^{-1}, 350–573 K),[48] $KMnInMo_3O_{12}$ (1.66×10^{-6} K^{-1}, 300–900 K),[49] $K_{0.5}Bi_{0.5}TiO_3$ (373–573 K),[50] and $CrVMoO_7$ (-1.92×10^{-6} K^{-1}, 100–240 K; 2.28×10^{-6} K^{-1}, 240–473 K).[51]

The temperature dependence of bond angles was analyzed to investigate the NTE mechanism of $Sc_{1.6}(MgTi)_{0.2}Mo_3O_{12}$. As shown in Fig. 3c, the $Sc(Mg/Ti)O_6$ octahedra and MoO_4 tetrahedra are connected by O atoms, forming intersecting chains within the ac plane. With increasing temperature, θ_1 (the $Sc(Mg/Ti)$–Mo_1–$Sc(Mg/Ti)$ angle) exhibits a notable decrease, whereas θ_2 (the $Sc(Mg/Ti)$–Mo_2–$Sc(Mg/Ti)$ angle) shows a slight increase (Fig. 3d). This structural adjustment leads to a contraction of the chain-like structure, corresponding to NTE along the ac
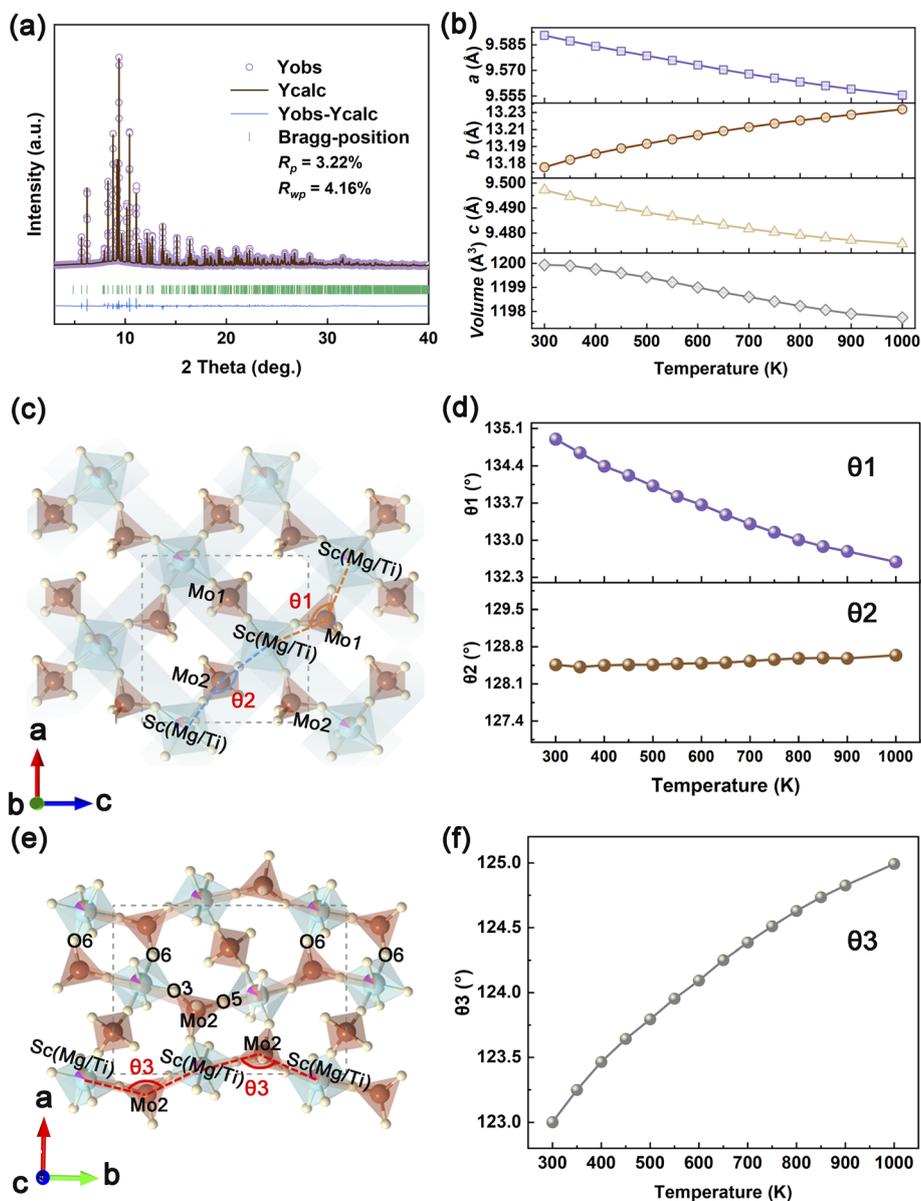

Fig. 3 (a) Refinement result of $Sc_{1.6}(MgTi)_{0.2}Mo_3O_{12}$ at 300 K. (b) Temperature dependence of lattice constants and unit cell volume. (c) Structure diagram of $Sc_{1.6}(MgTi)_{0.2}Mo_3O_{12}$ viewed along the b-axis. (d) Variation of dihedral angles θ_1 and θ_2 with temperature. (e) Structure diagram of $Sc_{1.6}(MgTi)_{0.2}Mo_3O_{12}$ viewed along the c-axis. (f) Variation of the dihedral angle θ_3 with temperature.

plane. Along the c-axis, Sc(Mg/Ti)O$_6$ octahedra and MoO$_4$ tetrahedra are bridged by O3 atoms, forming chains that extend along the b-axis (Fig. 3e), with adjacent chains connected by O6 atoms. The increase in θ_3 with temperature explains the expansion along the b-axis (Fig. 3f).

In$_2$Mo$_{2.5}$W$_{0.5}$O$_{12}$ is the second example, exhibiting $P2_1/c$ symmetry at room temperature. SXRD measurements were performed on In$_2$Mo$_{2.5}$W$_{0.5}$O$_{12}$ (300–1000 K) (Fig. S4). As the temperature increases to 600 K, the intensity of the characteristic peaks associated with the monoclinic phase significantly diminishes, and new peaks emerge at their shoulders. Upon further heating to 620 K, the characteristic peaks of the monoclinic phase disappear (Fig. S4). A phase transition from monoclinic to orthorhombic is indicated by Rietveld refinement of the SXRD data (Fig. 4a). Furthermore, a weak endothermic peak detected in the differential scanning calorimetry (DSC) curve at 600 K verifies the occurrence of the phase transition (Fig. S5 and Table S4). The monoclinic phase exhibits PTE, while the orthorhombic phase shows anisotropic thermal expansion behavior, with $\alpha_a = +5.12 \times 10^{-6}$ K^{-1}, $\alpha_b = -3.68 \times 10^{-6}$ K^{-1}, and $\alpha_c = -5.54 \times 10^{-6}$ K^{-1} (Fig. 4b and S6). Overall, the volume decreases with increasing temperature, with a volumetric CTE of -4.11×10^{-6} K^{-1} (Fig. 4b). Similar to Sc$_{1.6}$(MgTi)$_{0.2}$Mo$_3$O$_{12}$, the decrease in θ_1 and the slight increase in θ_2 contribute to the contraction of the b- and c-axes, while the increase in θ_3 is the primary driver of the PTE along the a-axis (Fig. S7).

As the third example, we designed and synthesized the high-entropy oxide (Al$_{0.2}$Sc$_{0.2}$Fe$_{0.2}$Ga$_{0.2}$Cr$_{0.2}$)$_2$W$_3$O$_{12}$. By analyzing the temperature-dependent diffraction peaks, we identified a phase transition from the monoclinic ($P2_1/c$) to the orthorhombic phase ($Pnca$) in (Al$_{0.2}$Sc$_{0.2}$Fe$_{0.2}$Ga$_{0.2}$Cr$_{0.2}$)$_2$W$_3$O$_{12}$ (Fig. 4c and S8, Table S5). As shown in Fig. 4d, the orthorhombic phase exhibits PTE, with a volumetric CTE of 3.63×10^{-6} K^{-1}. This behavior results from the combined effects of the a, b, and c axes ($\alpha_a = -1.89 \times 10^{-6}$ K^{-1}, $\alpha_b = +5.99 \times 10^{-6}$ K^{-1}, and $\alpha_c = -0.52 \times 10^{-6}$ K^{-1}). The thermal expansion behavior of (Al$_{0.2}$Sc$_{0.2}$Fe$_{0.2}$Ga$_{0.2}$Cr$_{0.2}$)$_2$W$_3$O$_{12}$ can also be explained in terms of its crystal structure. As illustrated in Fig. S11, as the temperature increases, variations in θ_1, θ_2, and θ_3 correspond to contraction along the a and c axes and expansion along the b axis.

In summary, returning to the concept of CII, it is proposed as a perspective for understanding how to control and design the CTE in framework materials. The precise regulation of thermal expansion indeed remains a key scientific challenge. Although NTE has been explored in recent years, our ability to control thermal expansion is still limited.[8] In framework compounds, it is well accepted that structural flexibility determines thermal expansion.[34] In this work, we found that the CII can reflect structural flexibility. Thus, we adopt this idea to quantify and design CTE based on chemical composition. The relationship between CII and thermal expansion seems to be more distinct than that between AAV and thermal expansion, at least for the family of A$_2$M$_3$O$_{12}$ compounds investigated here. First, using the A$_2$M$_3$O$_{12}$ system, where more experimental thermal expansion data are available, we identified a critical CII value of about 2.64 Å^{-2}, below which NTE occurs, and above which PTE is observed. Further theoretical calculations also indicate that
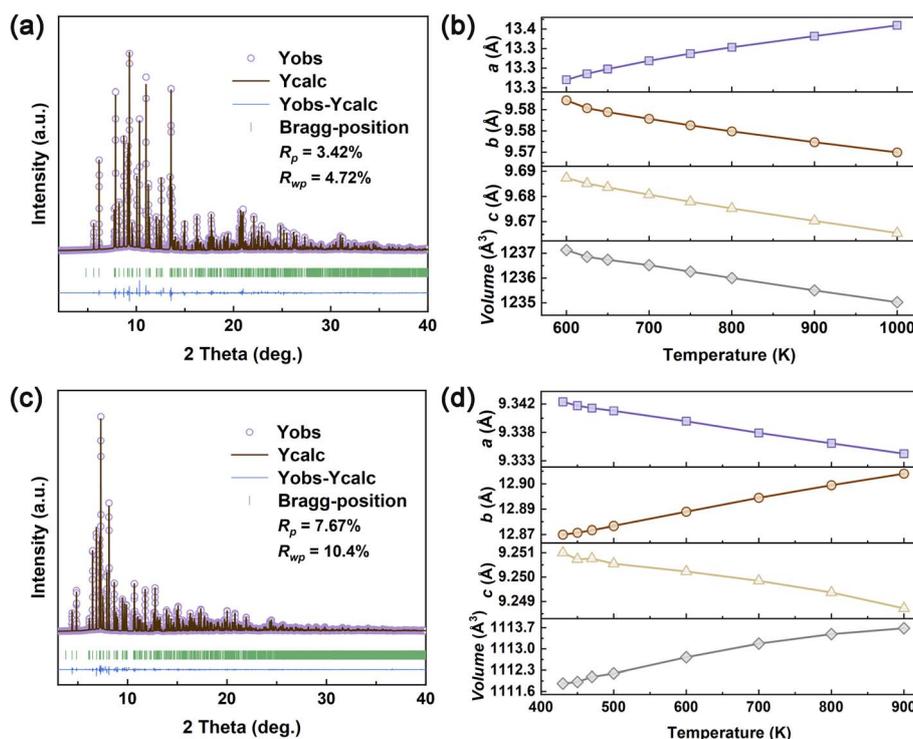

Fig. 4 (a) Rietveld refinement of SXRD data for In$_2$Mo$_{2.5}$W$_{0.5}$O$_{12}$ at 620 K. (b) Temperature dependence of the lattice constants and volume in the 600–1000 K range. (c) Rietveld refinement of SXRD data for (Al$_{0.2}$Sc$_{0.2}$Fe$_{0.2}$Ga$_{0.2}$Cr$_{0.2}$)$_2$W$_3$O$_{12}$ at 430 K. (d) Temperature dependence of the lattice constants and volume in the 430–900 K range.

a smaller CII correlates with reduced energy required for the transverse shift of bridging O atoms, leading to more low-frequency phonon modes with negative Grüneisen parameters. Second, we designed three representative experimental examples: $Sc_{1.6}(MgTi)_{0.2}Mo_3O_{12}$, $In_2Mo_{2.5}W_{0.5}O_{12}$, and $(Al_{0.2}Sc_{0.2}Fe_{0.2}Ga_{0.2}Cr_{0.2})_2W_3O_{12}$, which exhibited volumetric CTE values of -2.11×10^{-6} K^{-1}, -4.10×10^{-6} K^{-1}, and $+3.63 \times 10^{-6}$ K^{-1}, respectively. These values closely match the CTE predictions based on the CII (-1.87×10^{-6} K^{-1}, -5.12×10^{-6} K^{-1}, and $+3.64 \times 10^{-6}$ K^{-1}), providing strong evidence of its effectiveness.

The CII concept incorporates the effects of ionic radii and charge, similar to bond strength. However, when applied to other systems, the critical value may vary due to differences in ionic radii, limiting its universality. Additionally, crystal symmetry plays a crucial role in structural flexibility.[52] It is important to note that the $A_2M_3O_{12}$ system studied here has the same orthorhombic phase. Therefore, when extending the CII idea to other oxide systems, symmetry must also be considered. For example, the CTE of α-HfW_2O_8 is -26.4×10^{-6} K^{-1} (90–468 K), whereas that of β-HfW_2O_8 is -16.5×10^{-6} K^{-1} (468–560 K),[53] highlighting the influence of crystal symmetry. The current CII concept is based on the role of bridging O atoms and may also be applicable to other systems, such as fluorides or cyanides. It should be noted that this concept of CII is not applied to the role of guest insertion (CO_2 and CCl_4) in the thermal expansion. The original intention of the concept of CII is to design and assess the coefficient of thermal expansion in framework materials rapidly, based on the chemical composition. In this work, we used the $A_2M_3O_{12}$ system as a case study to establish the relationship between the CII and thermal expansion. We hope that future developments of the CII concept will integrate all framework compounds, ultimately serving as a more general parameter for guiding the precise regulation of thermal expansion in these materials.

Conclusion

This work introduces the CII as a strategic parameter for achieving precise control over thermal expansion in open-framework $A_2M_3O_{12}$ materials. A strong structure–property relationship was identified between CII values and CTE, where a larger CII value corresponds to a more pronounced NTE effect. First principles calculations on $Al_2Mo_3O_{12}$, $Sc_2Mo_3O_{12}$, and $Y_2Mo_3O_{12}$ were conducted to investigate the underlying factors influencing their thermal expansion behavior, validating the CII concept from a theoretical perspective. By analyzing the transverse movement of O atoms, the potential wells were calculated, revealing the ease of lateral atomic vibrations. $Y_2Mo_3O_{12}$, with the smallest CII value, exhibits the flattest potential well curve, facilitating transverse O vibrations and aligning with its strong NTE behavior. Additionally, the Grüneisen parameters of all phonon modes indicate that $Y_2Mo_3O_{12}$ has more vibrational modes contributing to NTE compared to $Al_2Mo_3O_{12}$ and $Sc_2Mo_3O_{12}$, further elucidating the observed differences in their thermal expansion behavior. To further validate the CII idea, $Sc_{1.6}(MgTi)_{0.2}Mo_3O_{12}$, $In_2Mo_{2.5}W_{0.5}O_{12}$, and

$(Al_{0.2}Sc_{0.2}Fe_{0.2}Ga_{0.2}Cr_{0.2})_2W_3O_{12}$ were synthesized and characterized. Their thermal expansion behavior was studied using variable-temperature synchrotron XRD, which confirms that $In_2Mo_{2.5}W_{0.5}O_{12}$, with the smallest CII value, exhibits NTE behavior, while $(Al_{0.2}Sc_{0.2}Fe_{0.2}Ga_{0.2}Cr_{0.2})_2W_3O_{12}$, with the largest CII value, exhibits PTE. This work establishes the CII as a useful parameter for estimating the potential for transverse thermal vibrations in bridge-chain atoms, offering a new approach for the precise regulation of NTE in framework materials.

Author contributions

Qilong Gao initiated and designed the research. Xin Chen synthesized the samples and measured and analysed the SXRD data. Kaiyue Zhao and Qiang Sun performed the first principles calculations. Yongqiang Qiao, Juan Guo and Shogo Kawaguchi measured and helped to analyse the data. Andrea Sanson, Erjun Liang and Jun Chen discussed and commented on the manuscript. Qilong Gao, Xin Chen and Andrea Sanson discussed and wrote the manuscript. Qilong Gao guided the projects.

Conflicts of interest

The authors declare no competing financial interests.

Data availability

The data that support the findings of this study are available from the corresponding author upon reasonable request.

Supplementary information includes details of the experiment and calculation, variable temperature SXRD data, TG and DSC data, ionic radii used in the paper, the calculated CII value, and the structure parameters. See DOI: **https://doi.org/10.1039/d5sc03604f**.

Notes and references

1 J. S. O. Evans, *J. Chem. Soc., Dalton Trans.*, 1999, **19**, 3317–3326.

2 K. Takenaka, *Sci. Technol. Adv. Mater.*, 2012, **13**, 013001.

3 M. Azuma, W. T. Chen, H. Seki, M. Czapski, S. Olga, K. Oka, M. Mizumaki, T. Watanuki, N. Ishimatsu, N. Kawamura, S. Ishiwata, M. G. Tucker, Y. Shimakawa and J. P. Attfield, *Nat. Commun.*, 2011, **2**, 1361.

4 K. Takenaka, Y. Okamoto, T. Shinoda, N. Katayama and Y. Sakai, *Nat. Commun.*, 2017, **8**, 14102.

5 C. Wang, L. H. Chu, Q. R. Yao, Y. Sun, M. M. Wu, L. Ding, J. Yan, Y. Y. Na, W. H. Tang, G. N. Li, Q. Z. Huang and J. W. Lynn, *Phys. Rev. B: Condens. Matter Mater. Phys.*, 2012, **85**, 220103(R).

6 S. H. Lohaus, M. Heine, P. Guzman, C. M. Bernal-Choban, C. N. Saunders, G. Shen, O. Hellman, D. Broido and B. Fultz, *Nat. Phys.*, 2023, **19**, 1642–1648.

7 G. Ernst, C. Broholm, G. R. Kowach and A. P. Ramirez, *Nature*, 1998, **396**, 147–149.

8 N. K. Shi, Y. Z. Song, X. R. Xing and J. Chen, *Coord. Chem. Rev.*, 2021, **449**, 214204.

9 M. T. Dove and H. Fang, *Rep. Prog. Phys.*, 2016, **79**, 066503.

10 X. L. Yuan, B. Wang, Y. Sun, H. M. Guo, K. W. Shi, S. H. Deng, L. H. He, H. Q. Lu, H. Zhang, S. D. Xu, Y. Du, W. C. Hao, S. Q. Chu, Z. J. Ma, S. H. An, J. Cui, D. M. Hu, H. M. Han and C. Wang, *Adv. Funct. Mater.*, 2024, **34**, 2404629.

11 J. P. Attfield, *Front. Chem.*, 2018, **6**, 00371.

12 E. J. Liang, Q. Sun, H. L. Yuan, J. Q. Wang, G. J. Zeng and Q. L. Gao, *Front. Phys.*, 2021, **16**(5), 53302.

13 M. Azuma, K. Oka and K. Nabetani, *Sci. Technol. Adv. Mater.*, 2015, **16**, 034904.

14 V. Crisan, P. Entel, H. Ebert, H. Akai, D. D. Johnson and J. B. Staunton, *Phys. Rev. B: Condens. Matter Mater. Phys.*, 2002, **66**, 014416.

15 A. V. Ruban, S. Khmelevskyi, P. Mohn and B. Johansson, *Phys. Rev. B: Condens. Matter Mater. Phys.*, 2007, **76**, 014420.

16 K. Takenaka and H. Takagi, *Appl. Phys. Lett.*, 2005, **87**, 261902.

17 R. J. Huang, Y. Y. Liu, W. Fan, J. Tan, F. R. Xiao, L. H. Qian and L. F. Li, *J. Am. Chem. Soc.*, 2013, **135**, 11469–11472.

18 Y. W. Long, N. Hayashi, T. Saito, M. Azuma, S. Muranaka and Y. Shimakawa, *Nature*, 2009, **458**, 60–63.

19 Z. Pan, Y. W. Fang, T. Nishikubo, L. Hu, S. Kawaguchi and M. Azuma, *Chem. Mater.*, 2022, **34**, 2798–2803.

20 T. A. Mary, J. S. O. Evans, T. Vogt and A. W. Sleight, *Science*, 1996, **272**, 90–92.

21 B. K. Greve, K. L. Martin, P. L. Lee, P. J. Chupas, K. W. Chapman and A. P. Wilkinson, *J. Am. Chem. Soc.*, 2010, **132**, 15496–15498.

22 A. L. Goodwin, M. Calleja, M. J. Conterio, M. T. Dove, J. S. O. Evans, D. A. Keen, L. Peters and M. G. Tucker, *Science*, 2008, **319**, 794–797.

23 J. C. Hancock, K. W. Chapman, G. J. Halder, C. R. Morelock, B. S. Karlan, L. C. Gallington, A. Bongiorno, C. Han, S. Zhou and A. P. Wilkinson, *Chem. Mater.*, 2015, **27**, 3912–3918.

24 N. Lock, Y. Wu, M. Christensen, L. J. Cameron, V. K. Peterson, A. J. Bridgeman, C. J. Kepert and B. B. Iversen, *J. Phys. Chem. C*, 2010, **114**, 16181–16186.

25 V. Korthuis, N. Khosrovani, A. W. Sleight, N. Roberts, R. Dupree and W. W. Warren, *Chem. Mater.*, 1995, **7**, 412–417.

26 K. W. Chapman, P. J. Chupas and C. J. Kepert, *J. Am. Chem. Soc.*, 2006, **128**, 7009–7014.

27 C. De Meyer, F. Bouree, J. S. O. Evans, K. De Buysser, E. Bruneel, I. Van Driessche and S. Hoste, *J. Mater. Chem.*, 2004, **14**, 2988–2994.

28 N. Nakajima, Y. Yamamura and T. Tsuji, *Solid State Commun.*, 2003, **128**, 193–196.

29 Y. Yamamura, K. Masago, M. Kato and T. Tsuji, *J. Phys. Chem. B*, 2007, **111**, 10118–10122.

30 J. Chen, Q. L. Gao, A. Sanson, X. X. Jiang, Q. Z. Huang, A. Carnera, C. G. Rodriguez, L. Olivi, L. Wang, L. Hu, K. Lin, Y. Ren, Z. S. Lin, C. Wang, L. Gu, J. X. Deng, J. P. Attfield and X. R. Xing, *Nat. Commun.*, 2017, **8**, 14441.

31 A. E. Phillips, A. L. Goodwin, G. J. Halder, P. D. Southon and C. J. Kepert, *Angew. Chem., Int. Ed.*, 2008, **47**, 1396–1399.

32 J. E. Auckett, A. A. Barkhordarian, S. H. Ogilvie, S. G. Duyker, H. Chevreau, V. K. Peterson and C. J. Kepert, *Nat. Commun.*, 2018, **9**, 4873.

33 A. Sanson, *Mater. Res. Lett.*, 2019, **7**, 412–417.

34 Q. L. Gao, J. Q. Wang, A. Sanson, Q. Sun, E. J. Liang, X. R. Xing and J. Chen, *J. Am. Chem. Soc.*, 2020, **142**, 6935–6939.

35 H. L. Yuan, C. Y. Wang, Q. L. Gao, G. J. Zeng, J. Guo, M. J. Chao, S. Kawaguchi, Y. Jia and E. J. Liang, *Mater. Horiz.*, 2021, **8**, 2562–2568.

36 Q. L. Gao, Y. X. Jiao, Q. Sun, J. A. P. Sprenger, M. Finze, A. Sanson, E. J. Liang, X. R. Xing and J. Chen, *Angew. Chem., Int. Ed.*, 2024, **63**, e202401302.

37 L. Hu, J. Chen, A. Sanson, H. Wu, C. G. Rodriguez, L. Olivi, Y. Ren, L. L. Fan, J. X. Deng and X. R. Xing, *J. Am. Chem. Soc.*, 2016, **138**, 8320–8323.

38 E. A. Harbourne, H. Barker, Q. Guéroult, J. Cattermull, L. A. V. Nagle-Cocco, N. Roth, J. S. O. Evans, D. A. Keen and A. L. Goodwin, *Chem. Mater.*, 2024, **36**, 5796–5804.

39 P. Meng, A. Brock, X. D. Wang, Y. T. Wang, J. McMurtrie and J. S. Xu, *Inorg. Chem. Front.*, 2023, **10**, 2399–2403.

40 A. K. A. Pryde, K. D. Hammonds, M. T. Dove, V. Heine, J. D. Gale and M. C. Warren, *J. Phys.: Condens. Matter*, 1996, **8**, 10973–10982.

41 A. Sanson, *Chem. Mater.*, 2014, **26**, 3716–3720.

42 R. D. Shannon, *Acta Crystallogr.*, 1976, **A32**, 751–767.

43 R. D. Shannon and C. T. Prewitt, *Acta Crystallogr.*, 1969, **B25**, 925–946.

44 M. Ari, P. M. Jardim, B. A. Marinkovic, F. Rizzo and F. F. Ferreira, *J. Solid State Chem.*, 2008, **181**, 1472–1479.

45 J. S. O. Evans and T. A. Mary, *Int. J. Inorg. Mater.*, 2000, **2**, 143–151.

46 C. Guzman-Afonso, C. Gonzalez-Silgo, J. Gonzalez-Platas, M. Eulalio Torres, A. Diego Lozano-Gorrin, N. Sabalisck, V. Sanchez-Fajardo, J. Campo and J. Rodriguez-Carvajal, *J. Phys.: Condens. Matter*, 2011, **23**, 325402.

47 J. C. Luo, K. X. Zou, B. Wang, X. L. Yuan, S. H. An, Z. J. Ma, K. W. Shi, S. H. Deng, J. P. Xu, W. Yin, W. H. Wang, C. Wang and Y. Sun, *Adv. Funct. Mater.*, 2024, **34**, 2410608.

48 Y. Q. Qiao, S. Zhang, P. X. Zhang, J. Guo, A. Sanson, X. Zhen, K. Y. Zhao, Q. L. Gao and J. Chen, *Nano Res.*, 2024, **17**, 2195–2203.

49 Q. J. Wang, Y. Q. Qiao, K. Y. Zhao, P. X. Zhang, H. Zhao, J. Guo, X. W. Shi, E. J. Liang and Q. L. Gao, *Acta Mater.*, 2024, **281**, 120358.

50 G. Das Adhikary, P. Punetha, R. P. Singh, V. Dwij, V. Sathe, A. Senyshyn, P. Nukala and R. Ranjan, *Phys. Rev. B*, 2023, **108**, L140104.

51 N. K. Shi, X. Q. Kong, A. Sanson, N. Wang, A. Venier, D. O. de Souza and J. Chen, *Scr. Mater.*, 2023, **235**, 115597.

52 Q. L. Gao, Y. X. Jiao, J. A. P. Sprenger, M. Finze, A. Sanson, Q. Sun, E. J. Liang and J. Chen, *J. Am. Chem. Soc.*, 2024, **146**, 21710–21720.

53 Y. Yamamura, N. Nakajima and T. Tsuji, *Phys. Rev. B: Condens. Matter Mater. Phys.*, 2001, **64**, 184109.